International Journal of Thermophysics, Vol. 22, No. 5, September 2001 (© 2001)

Radiative and Optical Properties of $La_{1-x}Sr_xMnO_3$ ($0 \leqslant x \leqslant 0.4$) in the Vicinity of Metal–Insulator Transition Temperatures from 173 to 413 K [1]

K. Shimazaki,[2,3] S. Tachikawa,[4] A. Ohnishi,[4] and Y. Nagasaka[5]

Radiative and optical properties of polycrystalline $La_{1-x}Sr_xMnO_3$ ($0 \leqslant x \leqslant 0.4$) in the vicinity of the metal–insulator transition are presented. The temperature dependence of the total hemispherical emittance ε_H of $La_{1-x}Sr_xMnO_3$ was measured by the calorimetric method in the temperature range from 173 to 413 K. It was confirmed that ε_H showed unexpected variation as a result of changes in the hole concentration (x). Especially in the case of $La_{0.825}Sr_{0.175}MnO_3$, ε_H remains high above the transition temperature T_C due to insulator-like behavior; on the other hand, it decreases sharply below T_C because of metallic behavior. The spectral reflectance was measured by FT-IR in the wavelength range of 0.25 to 100 μm at room temperature. The optical constants were calculated by Kramers–Kronig analysis of the spectral reflectance data. An insulator-like character of the optical properties appears at lower Sr^{2+} doping levels while a metallic one exists at higher Sr^{2+} doping levels.

KEY WORDS: Kramers–Kronig analysis; $La_{1-x}Sr_xMnO_3$; manganese oxide; optical constants; perovskite; spectral reflectance; total hemispherical emittance.

1. INTRODUCTION

To maintain the desired temperature of the spacecraft for all mission phases, a wide variety of thermal control materials or devices has been

[1] Paper presented at the Fourteenth Symposium on Thermophysical Properties, June 25–30, 2000, Boulder, Colorado, U.S.A.

[2] Graduate School of Science and Technology, Keio University, 3-14-1, Hiyoshi, Yokohama 223-8522, Japan.

[3] To whom correspondence should be addressed. E-mail: kazunori@pub.isas.ac.jp

[4] The Institute of Space and Astronautical Science, 3-1-1, Yoshinodai, Sagamihara 229-8510, Japan.

[5] Department of System Design Engineering, Keio University, 3-14-1, Hiyoshi, Yokohama 223-8522, Japan.

0195-928X/01/0900-1549/0 © 2001 Plenum Publishing Corporation

used. Recently the development of new thermal control materials for spacecraft has become a priority due to need of the density and efficiency of the instruments on the spacecraft to grow. It is important to know the thermal radiative and optical properties of such newly developed thermal control materials. As a new thermal control material, we have employed $La_{1-x}Sr_xMnO_3$, manganese oxide with a perovskite-type structure, which can be obtained from $LaMnO_3$ by substitution of La^{3+} ions with Sr^{2+} ones. These perovskite-type manganites have attracted much attention because of their phenomenal magnetic and transport properties. In particular, giant magnetoresistance phenomena and metal-insulator transitions have been widely observed as long as the Mn^{4+}/Mn^{3+} mixed valence ratio is in the appropriate range [1–3]. The mechanism of the ferromagnetic transition and the coincident metal–insulator transition has been traditionally understood on the basis of the double-exchange interaction model [4–7]. More recent theoretical and experimental studies pointed out the importance of the electron–phonon interaction, known by the name "polaron," which relates to Jahn–Teller-type lattice distortions of the MnO_6 octahedra [8, 9], in addition to the double-exchange interaction.

Here we present the radiative and optical properties of $La_{1-x}Sr_xMnO_3$ in the vicinity of the metal–insulator transition temperatures. They show various changes depending on its temperature and molar ratio of Sr^{2+}. The temperature dependence of the total hemispherical emittance ε_H was measured by the calorimetric method between 173 and 413 K. The spectral reflectance was measured by FT-IR in the wavelength range of 0.25 to 100 μm at room temperature to investigate the influence of the Sr^{2+} doping level on the optical properties. The optical constants, refractive index n, and extinction coefficient k, which determine the radiative and optical properties, were calculated by Kramers–Kronig (K-K) analysis of the spectral reflectance data. The absorption coefficient A was calculated using k.

2. SAMPLES AND CHARACTERIZATION

Polycrystalline $La_{1-x}Sr_xMnO_3$ ($x=0$, 0.15, 0.175, 0.2, 0.3, and 0.4) test samples were selected and prepared using the standard ceramic production process [10]. The dimensions of the sample are nearly $30\times30\times0.2$ mm. The surfaces of every sample were polished by diamond slurry. The surface roughness of the sample was measured by a surface roughness measuring instrument (Tokyo Seimitsu Co., Ltd.; Surfcom 130A). The root-mean-square roughness of the sample was under 30 nm.

As the hole concentration (x) is increased, $La_{1-x}Sr_xMnO_3$ shows some phase changes [3]. The parent material $LaMnO_3$ is an antiferromagnetic

insulator. For doping levels $0.1 \leqslant x \leqslant 0.17$, the phase changes from a paramagnetic insulator to a ferromagnetic insulator state with decreasing temperature. The ferromagnetic metal phase appears above $x \approx 0.17$ and the ferromagnetic transition temperature T_C exists near room temperature. Namely, a rapid reduction of the electronic resistivity begins at T_C and the metal phase turns up at a low temperature; this is the so-called metal–insulator transition. And above $x \approx 0.25$, the phase changes from a paramagnetic metal state to a ferromagnetic metal one as the temperature is reduced. Hence, it is speculated that the radiative and optical properties of $La_{1-x}Sr_xMnO_3$ show considerable variations in the vicinity of the metal–insulator transition.

3. TOTAL HEMISPHERICAL EMITTANCE ε_H

The total hemispherical emittance ε_H was measured by the calorimetric method. A detailed explanation of the calorimetric method and description of the measurement system will be published elsewhere [11]. The uncertainty of the present ε_H measurement was estimated to be, at most, $\pm 2.2\%$.

Figure 1 shows the results obtained in the present measurements for ε_H of $La_{1-x}Sr_xMnO_3$ ($x = 0$, 0.15, 0.175, 0.2, 0.3, and 0.4) in the temperature range from 173 to 413 K. The temperature dependence of ε_H in $La_{1-x}Sr_xMnO_3$ shows distinct behavior upon varying the doping level of Sr^{2+}. $LaMnO_3$ is an insulator and does not show any phase changes in this

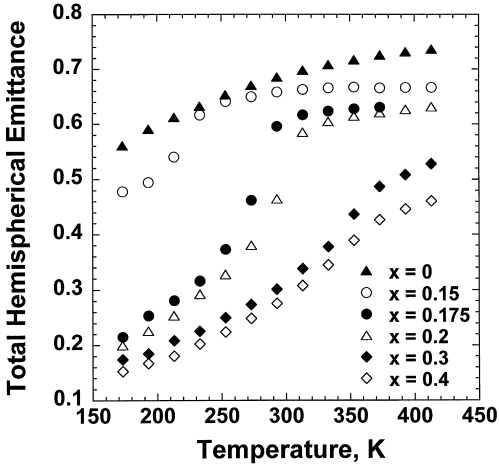

Fig. 1. Temperature dependence of the total hemispherical emittance ε_H in $La_{1-x}Sr_xMnO_3$ ($x = 0$, 0.15, 0.175, 0.2, 0.3, and 0.4).

temperature range [3]. Hence, no drastic change can be observed and ε_H shows a monotonic increase as a function of temperature. For $x = 0.15$, ε_H remains constant above 250 K and changes slightly as the paramagnetic–ferromagnetic insulator transition occurs below 250 K [3]. A similar result is obtained between $x = 0.175$ and $x = 0.2$, though the transition temperature and sharpness of the variation of ε_H are little different. These results indicate the unconventional features for thermal radiative properties of these samples. Namely, on the one hand, ε_H maintains its high value above T_C due to insulator-like behavior; on the other hand, it decreases sharply below T_C because of metallic behavior. The range of variation for ε_H is more than 0.40. This anomalous behavior of ε_H for $x = 0.175$ and 0.2 is ascribed to the significant change of the infrared reflectance: the phonon structures in the infrared region disappear due to the effect of dielectric screening, which is the result of the increased mobility of free electrons in the metal state [12, 13]. For $x = 0.3$ and 0.4, the slope of the temperature dependence of ε_H changes slightly at the paramagnetic-ferromagnetic transition [3]. The ε_H for $x = 0.3$ and 0.4 is smaller than that for the other samples in the entire temperature range as the samples are in the metallic state over the whole temperature region.

Figure 2 shows the measured ε_H of $La_{1-x}Sr_xMnO_3$ ($x = 0$, 0.15, 0.175, 0.2, 0.3, and 0.4) at 293 K. The effect of Sr^{2+} doping on the ε_H is clearly visible. The total hemispherical emittance ε_H in the range $0 \leqslant x \leqslant 0.175$ is obviously different from that in the range $0.175 \leqslant x \leqslant 0.4$. In the vicinity of

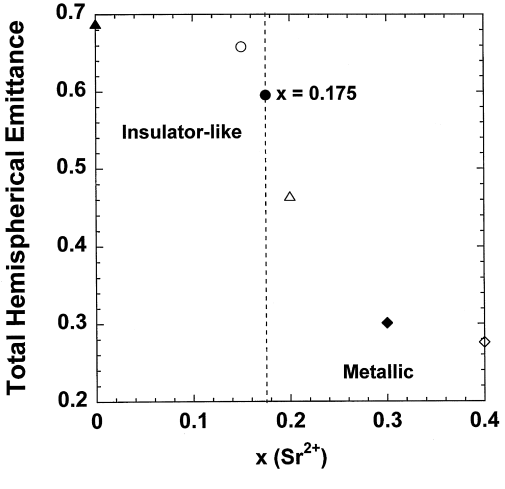

Fig. 2. Total hemispherical emittance in $La_{1-x}Sr_xMnO_3$ ($x = 0$, 0.15, 0.175, 0.2, 0.3, and 0.4) at 293 K.

$x = 0.175$, which is close to the nonmetal–metal compositional phase boundary [1], ε_H shows a remarkable variation caused by even slightly different Sr^{2+} doping. When the doping level is low, ε_H is large as can be expected for any nonmetal. As the doping level is increased whereas the mobility of the free electrons grows, ε_H gradually decreases to reach values characteristic for metals. The reason for the room temperature dependence of ε_H on doping is discussed in Section 4.3.

4. OPTICAL PROPERTIES

4.1. Experimental and Kramers–Kronig Analysis

Spectral reflectance with near-normal incidence was measured for $La_{1-x}Sr_xMnO_3$ ($x = 0$, 0.15, 0.175, 0.2, 0.3, and 0.4) at room temperature. Spectral reflectance in the wavelength region of 0.25 to 100 μm was measured using Fourier-transform spectroscopy (Bio-Rad; FTS-60A/896). As a reference, we used an aluminum mirror. The optical constants, refractive index n and extinction coefficient k, were calculated by Kramers–Kronig (K-K) analysis [14] of the spectral reflectance data. At a near-normal-incidence angle, n and k are given by

$$n = \frac{1-R}{1+R-2\sqrt{R}\cos\theta} \tag{1}$$

$$k = \frac{-2\sqrt{R}\sin\theta}{1+R-2\sqrt{R}\cos\theta} \tag{2}$$

where R is the experimentally observed spectral reflectance (single surface reflection). The quantities n, k, and R are functions of the frequency, which is omitted to simplify the expressions in Eqs. (1) and (2). The phase difference θ between the incident and the reflected waves is obtained from the following relation:

$$\theta(\omega_i) = -\frac{\omega_i}{\pi}\int_0^\infty \frac{\ln[R(\omega)/R(\omega_i)]}{\omega^2-\omega_i^2}\,d\omega \tag{3}$$

Here, $\theta(\omega_i)$ is the value of the phase difference at frequency ω_i. The integral is evaluated numerically. Extrapolations of the spectral reflectance to high and low frequencies are required since the measured spectral range

is finite. For the analysis we assumed a constant reflectance from 0.25 to 0.1 μm and $R \propto \omega^{-4}$ extrapolation below 0.1 μm. Depending on the electronic states, the reflectance extrapolations above 100 μm were the constant reflectance or the reflectance described by the Hagen–Rubens relation $(1-R) \propto \sqrt{\omega}$. The absorption coefficient is given by [15]

$$A = \frac{4\pi}{\lambda} k \tag{4}$$

where λ is the wavelength.

4.2. Discussion of the Data Calculated by K-K Analysis

To investigate the K-K analysis error due to the uncertainty in the extrapolation of the spectral reflectance from zero to infinity, we perform analytical dispersion analysis of the measured spectral reflectance. A model based on the following factorized expression of the complex dielectric function is applied [16]:

$$\hat{\varepsilon}(\omega) = \varepsilon_1 + i\varepsilon_2 = \varepsilon_\infty \prod_j \frac{\omega^2 - \omega_{Lj}^2 + i\gamma_{Lj}\omega}{\omega^2 - \omega_{Tj}^2 + i\gamma_{Tj}\omega} \tag{5}$$

The adjustable parameters, the high-frequency dielectric constant ε_∞ and the frequencies ω_{Tj} and ω_{Lj} and damping terms γ_{Tj} and γ_{Lj} for the jth transverse optical (TO)–longitudinal optical (LO) pair, are uniquely determined. Thus, ε_1 and ε_2 are the real and imaginary parts of the complex dielectric constants, respectively. The band contour described by the factorized model is similar to that by the classical analytical model for the complex dielectric constant. The model has been successfully used to fit infrared spectral reflectance of several perovskite oxides [17, 18]. The factorized model has four free parameters per oscillator instead of three as in the classical model, so it is much more flexible than the classical model.

The spectral reflectance is expressed by Eq. (6), using ε_1 and ε_2. We perform curve fitting with Eqs. (5) and (6). The simplex method [19] is employed for curve fitting.

$$R = \frac{\sqrt{(\varepsilon_1^2 + \varepsilon_2^2)} - \sqrt{2(\varepsilon_1 + \sqrt{\varepsilon_1^2 + \varepsilon_2^2})} + 1}{\sqrt{(\varepsilon_1^2 + \varepsilon_2^2)} + \sqrt{2(\varepsilon_1 + \sqrt{\varepsilon_1^2 + \varepsilon_2^2})} + 1} \tag{6}$$

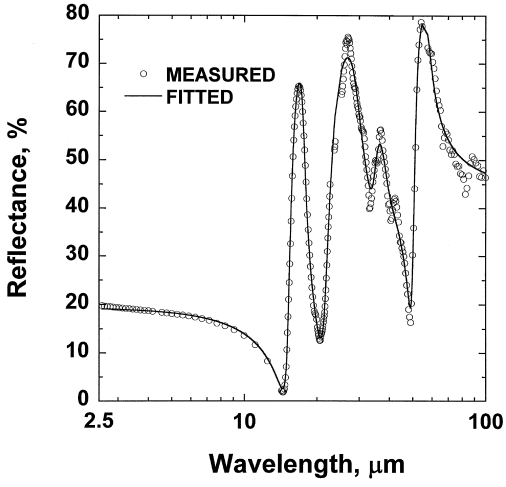

Fig. 3. Spectral reflectance of $LaMnO_3$. (○): measured data; (——): fitting curve from Eqs. (5) and (6).

Representing the $La_{1-x}Sr_xMnO_3$ system, the result of curve fitting to the spectral reflectance of $LaMnO_3$ is shown in Fig. 3. The open circles show the measured spectral reflectance; the solid curve is the fit to the data. The obtained fitting parameters are listed in Table I. A slight mismatch is observed near 30 μm between the measured spectral reflectance and the fitted value. However, the factorized model satisfactorily describes the outline of the spectrum of $LaMnO_3$ and agrees well with the measured reflectance. The standard deviation between the measured spectral reflectance and the fitted value is $\pm 3.9\%$.

Table I. Fitting Parameters of Eqs. (5) and (6) for $LaMnO_3$

j	1	2	3	4	5
ω_{Tj} (cm^{-1})	172.1	259.2	272.5	343.6	566.8
γ_{Tj}	13.7	53.4	31.6	43.4	28.8
ω_{Lj} (cm^{-1})	200.4	464.3	290.8	254.3	660.6
γ_{Lj}	10.1	50.1	34.2	42.8	41.4
ε_∞	6.6				

The optical constants are expressed by Eqs. (7) and (8), using ε_1 and ε_2.

$$n = \sqrt{\frac{1}{2}\left(\sqrt{\varepsilon_1^2 + \varepsilon_2^2} + \varepsilon_1\right)} \tag{7}$$

$$k = \sqrt{\frac{1}{2}\left(\sqrt{\varepsilon_1^2 + \varepsilon_2^2} - \varepsilon_1\right)} \tag{8}$$

The optical constants that yield the best fit to the reflectance data agree well with those calculated by K-K analysis as shown in Fig. 4. The standard deviation of the difference in optical constants obtained by K-K analysis and curve fitting is within ± 0.16. The results in the wavelength regions of 0.25 to 2.5 and 80 to 100 μm are omitted because it is inevitable that the error is large due to the nature of K-K analysis.

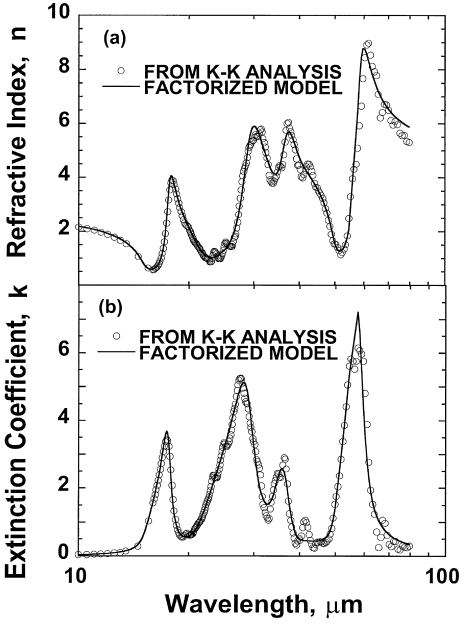

Fig. 4. Refractive index (a) and extinction coefficient (b) of $LaMnO_3$. (○): Calculated data from K-K analysis; (——):calculated by Eqs. (7) and (8) using the parameters in Table I.

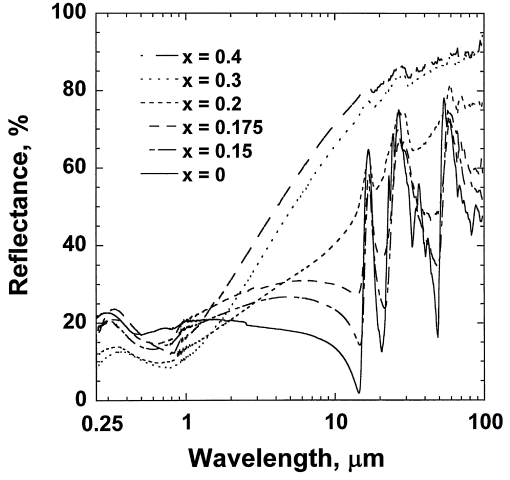

Fig. 5. Spectral reflectance of $La_{1-x}Sr_xMnO_3$ ($x = 0$, 0.15, 0.175, 0.2, 0.3, and 0.4) at room temperature.

4.3. Spectral Reflectance

Figure 5 shows the measured spectral reflectance for $La_{1-x}Sr_xMnO_3$ ($x = 0$, 0.15, 0.175, 0.2, 0.3, and 0.4) at room temperature. The distinct features of the spectral reflectance can be seen clearly. The spectral reflectance for $x = 0$ to 0.175 is characterized by the typical features of a nonmetal with sharp infrared peaks due to the transverse optical (TO) phonons at 17, 28, and 60 μm. A compound of the ideal cubic perovskite-type structure has three infrared-active phonon modes as shown in Fig. 6. Three strong TO phonon peaks correspond to the Mn–O stretching mode, Mn–O–Mn bending mode, and La-site external mode in ascending order of the wavelength [20, 21]. However, $LaMnO_3$ has more than three peaks in its optical

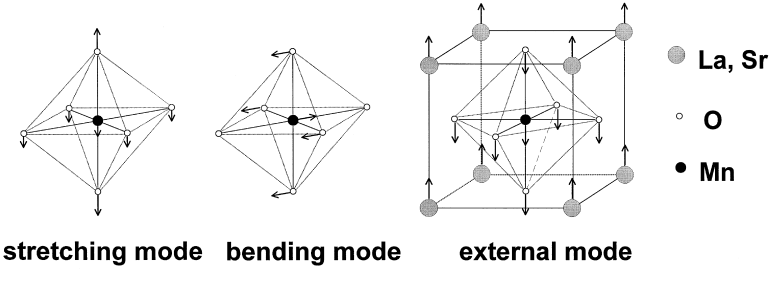

Fig. 6. Infrared-active vibration modes of the perovskite-type crystal structure.

spectrum since the lattice of $LaMnO_3$ is not ideally cubic but slightly distorted. The Mn–O–Mn bending mode is the most sensitive to lattice distortion of the MnO_6 octahedra [21].

No notable features can be seen under 1.0 μm, though there are small differences in magnitude of the spectral reflectance. Above 1.0 μm, the spectral reflectance for $x = 0.3$ and 0.4 is extremely different compared to that for $x = 0$. With increasing Sr^{2+} doping, the optical phonon peaks gradually disappear, accompanied by an increase in the spectral reflectance in the infrared region. Hence, the two compositions corresponding to $x = 0.3$ and 0.4 show metallic features in the optical spectrum rather than insulator-like ones. We believe that the reason the two compositions with $x = 0.3$ and 0.4 have such a high reflectance is that there is a contribution to the infrared optical phonons from free electrons whose mobility is increased with Sr^{2+} doping. In addition, the free carrier contribution screens the infrared optical phonon modes [12, 13]. Consequently, the variation in ε_H at room temperature as shown in Fig. 2 is attributed to the variation in the infrared spectral reflectance due to Sr^{2+} doping.

4.4. Optical Constants and Absorption Coefficient

Figure 7 represents the optical constants calculated by K-K analysis. The wavelength dependence of the optical constants for $x = 0$ to 0.2 is quite diverse. Generally there are three peaks except for the material with $x = 0$, for which the bending mode is split due to lattice distortion. As Sr^{2+} doping increases, it is observed that the three peaks gradually disappear, as well as the spectral reflectance. For the two compounds with $x = 0.3$ and 0.4 that are in the metallic state at room temperature, the optical constants do show metallic character and increase monotonically with the wavelength. The change in the optical constants from insulator-like to metallic behavior is accompanied by respective changes in the spectral reflectance. The changes in the spectral reflectance variation are attributable to the metal–insulator transition caused by Sr^{2+} doping, just as is the case with the optical constants.

The absorption coefficient A obtained from Eq. (4) is shown in Fig. 8. Like the spectral reflectance and optical constants, A varies from an insulator-like feature to a metallic one according to Sr^{2+} doping. The absorption coefficient A for $x = 0.4$ at 10 μm is nearly two orders of magnitude larger than that for $x = 0$. In the insulator-like state, strong absorption peaks due to the optical phonons appear at 17, 28, and 60 μm. In the metallic state, no obvious absorption peak can be seen and the wavelength dependence is weak. From these results, at low doping levels, it is verified that the electromagnetic waves penetrate into the materials to

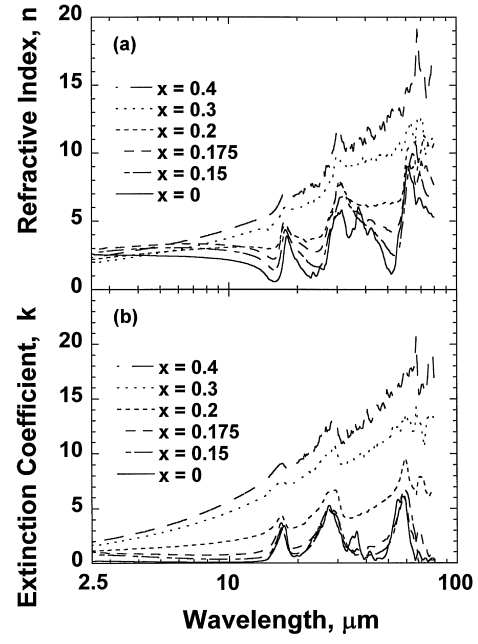

Fig. 7. Refractive index (a) and extinction coefficient (b) of $La_{1-x}Sr_xMnO_3$ ($x = 0$, 0.15, 0.175, 0.2, 0.3, and 0.4) at room temperature.

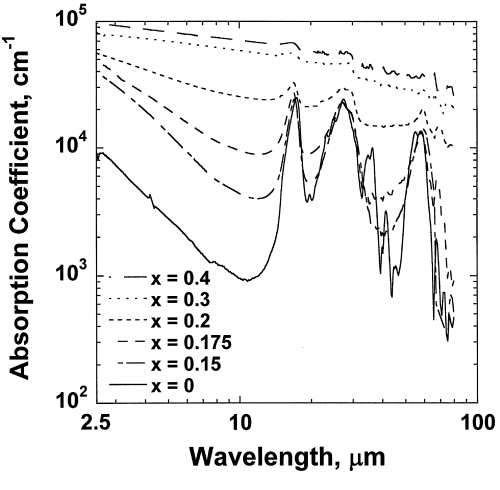

Fig. 8. Absorption coefficient of $La_{1-x}Sr_xMnO_3$ ($x = 0$, 0.15, 0.175, 0.2, 0.3, and 0.4) at room temperature.

a certain depth from the surface but are gradually absorbed by the optical phonons. On the other hand, at high doping levels, the electromagnetic waves are either reflected at the surface or absorbed in a relatively thin surface layer because, due to free electrons contribution, it is hard for the electromagnetic waves to penetrate.

5. CONCLUSIONS

The temperature dependence of the total hemispherical emittance ε_H of the $La_{1-x}Sr_xMnO_3$ system was measured in the temperature range from 173 to 413 K. It was found that ε_H depends on both the temperature and the Sr^{2+} doping. Moreover, the effect of Sr^{2+} doping on the optical properties was clarified. The optical constants were calculated by K-K analysis. The variation of the optical constants and the spectral reflectance is attributable to the metal–insulator transition due to Sr^{2+} doping.

$La_{1-x}Sr_xMnO_3$ has the potential for applications as a thermal control material in space because its radiative and optical properties can be controlled over a wide range.

ACKNOWLEDGMENTS

We thank A. Okamoto, Y. Nakamura, Y. Shimakawa, M. Kosaka, T. Mori, and A. Ochi of NEC Corporation for sample preparation.

REFERENCES

1. Y. Tokura, A. Urushibara, Y. Moritomo, T. Arima, A. Asamitsu, G. Kido, and N. Furukawa, *J. Phys. Soc. Jpn.* **63**:3931 (1994).
2. A. P. Ramirez, S.-W. Cheong, and P. Schiffer, *J. Appl. Phys.* **81**:5337 (1997).
3. A. Urushibara, Y. Moritomo, T. Arima, A. Asamitsu, G. Kido, and Y. Tokura, *Phys. Rev.* **51**:14103 (1995).
4. K. Kubo and N. Ohata, *J. Phys. Soc. Jpn.* **33**:21 (1972).
5. C. Zener, *Phys. Rev.* **81**:403 (1951).
6. P.-G. de Gennes, *Phys. Rev.* **118**:141 (1960).
7. P. W. Anderson and H. Hasegawa, *Phys. Rev.* **100**:675 (1955).
8. A. J. Millis, P. B. Littlewood, and B. I. Shraiman, *Phys. Rev. Lett.* **74**:5144 (1995).
9. H. Y. Hwang, S.-W. Cheong, P. G. Radaelli, M. Marezio, and B. Batlogg, *Phys. Rev. Lett.* **75**:914 (1995).
10. G. H. Jonker and J. H. van Santen, *Physica* **16**:337 (1950).
11. K. Shimazaki, S. Tachikawa, A. Ohnishi, and Y. Nagasaka, *High Temp. High Press.* (in press).
12. Y. Okimoto, T. Katsufuji, T. Ishikawa, A. Urushibara, T. Arima, and Y. Tokura, *Phys. Rev. Lett.* **75**:109 (1995).
13. K. H. Kim, J. Y. Gu, H. S. Choi, G. W. Park, and T. W. Noh, *Phys. Rev. Lett.* **77**:1877 (1996).

14. D. M. Roessler, *Br. J. Appl. Phys.* **16**:1119 (1965).
15. R. Siegel and J. R. Howell, *Thermal Radiation Heat Transfer*, 3rd ed. (Taylor & Francis, Washington, DC, 1992), pp. 524–525.
16. D. W. Berreman and F. C. Unterwald, *Phys. Rev.* **174**:791 (1968).
17. K. Kamarás, K.-L. Barth, F. Keilmann, R. Henn, M. Reedyk, C. Thomsen, J. Kircher, P. Richards, and J.-L. Stehlé, *J. Appl. Phys.* **78**:1235 (1995).
18. A. V. Boris, N. N. Kovaleva, A. V. Bazhenov, A. V. Samoilov, N.-C. Yen, and R. P. Vasquez, *J. Appl. Phys.* **81**:5756 (1997).
19. J. A. Nelder and R. Mead, *Comput. J.* **7**:308 (1965).
20. K. Nakamoto, *Infrared and Raman Spectra of Inorganic and Coordiation Compounds*, 4th ed. (Wiley, New York, 1986), pp. 147–155.
21. T. Arima and Y. Tokura, *J. Phys. Soc. Jpn.* **64**:2488 (1995).